
Original Paper

Investigation of Cavitation Models for Steady and Unsteady Cavitating Flow Simulation

Tan Dung Tran¹, Bernd Nennemann³, Thi Cong Vu³ and François Guibault²

¹Department of Mechanical Engineering, École Polytechnique de Montréal
2900 Boulevard Edouard-Montpetit, Montreal, H3T 1J4, Canada, tan-dung.tran@polymtl.ca

²Department of Computer and Software Engineering, École Polytechnique de Montréal
2900 Boulevard Edouard-Montpetit, Montreal, H3T 1J4, Canada, francois.guibault@polymtl.ca

³Andritz Hydro Canada Inc.
6100 Trans Canada Hwy, Pointe Claire, QC, H9R 1B9, Canada,
bernd.nennemann@andritz.com, thi.vu@andritz.com

Abstract

The objective of this paper is to evaluate the applicability of mass transfer cavitation models and determine appropriate numerical parameters for cavitating flow simulations. CFD simulations were performed for a NACA66 hydrofoil at cavitation numbers of 1.49 and 1.00, corresponding to steady sheet and unsteady sheet/cloud cavitating regimes using the Kubota and Merkle cavitation models. The Merkle model was implemented into CFX by User Fortran code. The Merkle cavitation model is found to give some improvements for cavitating flow simulation results for these cases. Turbulence modeling is also found to have an important contribution to the prediction quality of the simulations. The relationship between the turbulence viscosity modification, in order to take into account the local compressibility at the vapor/liquid interfaces, and the predicted numerical results is clarified. The limitations of current cavitating flow simulation techniques are discussed throughout the paper.

Keywords: Cavitation, CFD, steady, unsteady flow simulation, turbulence, cavitation local compressibility

1 Introduction

Cavitation is one of the main contributing factors to pressure fluctuations in hydraulic turbines which lead to noise, vibration and especially solid surface damage, usually called “cavitation erosion”. The focus of this paper is to evaluate different cavitation models which are applicable for the flow simulation of these machines. In order to evaluate the quality of the various existing cavitation models, it is important to study them on geometrically simple cases with well-documented, high-quality measurement data for validation.

The simulations are focused on the cavitating flow around a NACA66 hydrofoil for two different regimes: steady sheet cavitation and unsteady sheet/cloud cavitation which is well-known as one of the most complicated cavitation feature. A systematic study is performed for the influence of different RANS turbulence models, different mesh types, different distances from hydrofoil wall to first mesh node and different mesh expansions around the hydrofoil for different cavitation models. The aim is to predict the pressure fluctuations on the cavitating hydrofoil with a good numerical precision and to understand the influence of different cavitating regimes on the hydrofoil dynamics. The present work is an extension to the results presented in two recent ASME [1] and IAHR [2] conferences. The two transport-based cavitation models studied and presented in this paper are named here as the Kubota model and the Merkle model for simplicity. The Kubota model is the only model available in the CFX solver. The Merkle model is one of the most original cavitation models which is simple, robust and without consideration of thermodynamic effects. Therefore, we utilized the advantages of these isothermal cavitation models for the simulation of water/vapor cavitating flow around the hydrofoil where the thermal effect can be neglected. The Merkle model was implemented into the solver by Fortran programming code. The Kubota model was also implemented by Fortran code for methodology verification purposes.

Received January 15 2015; revised July 29 2015; accepted for publication October 15 2015: Review conducted by Prof. Yoshinobu Tsujimoto. (Paper number O15053S)

Corresponding author: Tan Dung Tran, tan-dung.tran@polymtl.ca

This paper was presented at the 27th IAHR Symposium on Hydraulic Machinery and Systems, September 4, Montreal, Canada.

2 State of the Art

Cavitation is a multiphase fluid phenomenon interplaying with the turbulence characteristics of the flow. It can happen in any type of fluid flow, under various forms, and can be both beneficial and destructive in daily life and industry. Due to its damaging effects in different fields such as mechanical, aeronautical, aerospace, chemical, and biomedical engineering, cavitation has attracted many researchers for over a century.

Numerous experimental tests have been carried out for two popular cases: hydrofoils [3-5] and Venturi sections [6, 7] to understand the physics of the cavitating flows. The characteristics of cavitation have been reported in several books and articles [8-10], describing various forms of cavitation where the unsteady sheet/cloud is one of the most complicated and destructive states for hydraulic machines. One of the earliest standard experimental reports found on this topic was written by Kubota et al. in 1989 [11]. They used Laser Doppler Anemometry (LDA) and high speed camera for measuring the unsteady cloud cavitation. Their results showed that the flow vorticity is at a maximum at the cloud center, surrounded by many small cavitation bubbles. Different other authors have used also the LDA, high speed camera and Particle Image Velocimetry (PIV) methods for measuring the cavitation dynamics at different regimes, at different operating conditions and on different foil geometries. Recently, Kravtsova et al. [12] presented their observation results on a hydrofoil NACA0015, and a semi-circular plate for studying the factors affecting cavitation inception and cavitation patterns. Their results show that cavitation inception depends on the flow development around the leading edge. And the subsequent cavitating flow pattern depends strongly on the operating conditions. Despite many interesting measurement studies realized on cavitation dynamics, the phenomenon is not yet fully understood due to its complexity related to: laminar/turbulent transition, detached/reattached bubbly flows, shear layers, phase-to-phase interface transfer and vortical structures [10, 13].

Due to the various limitations of measurement techniques, significant efforts have been made to develop accurate numerical methods for cavitating flow simulations in recent years. Examples of recent review articles on this topic can be found in [8, 10, 14, 15]. The selection of an appropriate model for cavitating flow simulation is very delicate. Most models assume the cavitating flow to be homogenous and isothermal. For solving the density of the liquid/vapor mixture in the cavitating flow, two main approaches are utilized: barotropic equation of state and transport equations. In the first approach proposed by Delannoy and Kueny in 1990, the local mixture density (ρ_m) is assumed to depend only on the local pressure: $\rho_m = f(p)$ in the barotropic equation of state [16, 17]. Recent experimental results showed that the vorticity is important in cavitating flow, particularly in the cavity closure region [18]. The production of this vorticity is the consequence of baroclinic torque:

$$\nabla \frac{1}{\rho_m} \times \nabla p \quad (1)$$

If the barotropic equation of state, $\rho_m = f(p)$, is used, the gradients of density and pressure are parallel, which leads to zero baroclinic torque. Hence, this approach is not able to simulate correctly the dynamics of cavitating flows [19].

The second approach has been developed based on transport equations to capture more detailed physical processes of cavitation involving bubble nucleation, growth, collapse, breakup, coalescence, and turbulent dispersion. In order to solve the local mixture density, a new transport equation is added into the transport equation system. To regulate the mass transfer between the liquid and vapor phases, various mathematical sources/sink terms representing the cavitation processes have been proposed [20-22]. The limitation of recent models in this approach is that no consideration is given to the slip at the interface between liquid and vapor phases.

In 1992, Kubota et al. [20] solved the Rayleigh-Plesset equation coupled with the RANS equations and with an assumed bubble radius for finding the local void fraction. Their proposed cavitation model is utilized nowadays in different CFD solvers. Later on, various authors have modified the source/sink cavitation terms from this model into different versions. To distinguish these different source/sink terms, each modified version is called a cavitation model followed by the name of the author who made the modification; for example, Kubota model, Merkle model, Kunz model, Singhal model, Senocak and Shyy model, etc. More than ten similar cavitation models can be found in different articles and reviews [15, 23]. But, very few studies on the comparison of these different cavitation models have been found, especially for the complicated regimes of cavitation such as: unsteady sheet/cloud cavitation or unsteady cloud cavitation. Merkle et al. in 1998 [24] and Kunz et al. in 2000 [21] introduced their model of source/sink cavitation terms corresponding to the evaporation and condensation processes for the cavity bubbles. They used an artificial compressibility method and a special preconditioning formulation for solving the Navier-Stokes transport equations with a RANS turbulence model. In 2002, Singhal et al. [22] presented their cavitation model called the "full-cavitation model" based on the rate of phase-change derived from a reduced form of the Rayleigh-Plesset equation for bubble dynamics and local flow conditions. This model is good for steady sheet or partial sheet cavitation cases, but for unsteady sheet/cloud cavitation cases, it has shown some difficulties in numerical convergence [25]. In 2003, Saito et al. [26] presented their cavitation model with consideration of thermal dynamic effects on the source/sink cavitation terms. The turbulent eddy viscosity was modified based on the Baldwin-Lomax model with the Degani-Schiff modification for solving the Navier-Stokes transport equations for the cavitating flow around a hydrofoil. They showed some very interesting results. Moreover, a few other authors have presented also cavitation models similar to those presented above but without thorough explanation of their modification [15, 23, 27]. Senocak and Shyy [28] presented the interface dynamics-based cavitation model. This model allows interpreting directly the empirical parameters in different existing cavitation models. This is an interesting idea, but this model currently only works for steady state simulations of cavitating flow. Young et al. [29] recently presented their work on the evaluation of cavitation models for the purposes of applying cavitating flow simulation for naval machines and fluid-structure interaction due to cavitation phenomenon. They have tested three cavitation models with some promising results. However, they have faced difficulties in numerical

convergence for the highly unsteady sheet/cloud cavitation regime.

Recently, a new four-equation cavitation model with consideration of thermodynamic effects has been presented by Goncalves et al. [30-32]. Their results showed that the new model performed well for sheet cavitation cases. For the strongly unsteady self-oscillating cavitation cases such as in transient sheet/cloud regime, the simulation results gave some promising results that could still be improved for precision and stability. This type of model requires more computational resources than other isothermal models.

In cavitating flow simulations, turbulence modeling is an important aspect due to the unstable nature of cavitation and the interaction between cavities and turbulent flow eddies. RANS turbulence models have been used to simulate various industrial fluid machines for years because of their good performance in giving acceptable simulation results within a reasonable computational time. For cavitating flow simulations, recent CFD studies showed that these turbulence models would need some modifications in the turbulent eddy viscosity [31, 33, 34]. There are several different RANS turbulence models for different utilities. However, few studies on the comparison of these different turbulence models for cavitation simulation have been found. Therefore, a systematic research on this topic is necessary. Recently, Large Eddy Simulation (LES) has been studied for unsteady cavitation simulations by a few researchers [35-37]. Some promising results have been obtained for some geometrically simplified cases. However, this method requires huge computational resources and it is not yet applicable industrially for CFD simulations.

3 Numerical Models

3.1 Conservation of Mass and Momentum

The steady Reynolds-averaged Navier–Stokes equations (RANS) are used to model the steady sheet cavitation case; and the unsteady RANS (URANS) equations are used to model the unsteady sheet/cloud cavitating regime case studied here. These conservation equations, for a Newtonian fluid without body forces and heat transfer, are presented below along with the mass transfer equation [38]:

$$\frac{\partial \rho_m}{\partial t} + \frac{\partial(\rho_m u_j)}{\partial x_j} = 0 \quad (2)$$

$$\frac{\partial(\rho_m u_i)}{\partial t} + \frac{\partial(\rho_m u_i u_j)}{\partial x_j} = -\frac{\partial p}{\partial x_i} + \frac{\partial}{\partial x_j} \left[(\mu_m + \mu_T) \left(\frac{\partial u_i}{\partial x_j} + \frac{\partial u_j}{\partial x_i} - \frac{2}{3} \frac{\partial u_k}{\partial x_k} \delta_{ij} \right) \right] \quad (3)$$

$$\frac{\partial(\rho_l \alpha_l)}{\partial t} + \frac{\partial(\rho_l \alpha_l u_j)}{\partial x_j} = \dot{m}^- - \dot{m}^+ \quad (4)$$

$$\rho_m = \rho_l \alpha_l + \rho_v \alpha_v \quad (5)$$

$$\mu_m = \mu_l \alpha_l + \mu_v \alpha_v \quad (6)$$

where ρ_m is the mixture density, ρ_l is the liquid density, ρ_v is the vapor density, α_v is the vapor fraction, α_l is the liquid fraction, u is the velocity, p is the pressure, μ_m is the mixture laminar viscosity, μ_l and μ_v are, respectively, the liquid and vapor dynamic viscosities, and μ_T is the turbulent viscosity. The subscripts (i , j , and k) denote the directions of the Cartesian coordinates. The source term \dot{m}^+ and the sink term \dot{m}^- represent the interphase mass transfer rates per unit volume for the condensation and evaporation processes, respectively.

3.2 Kubota Model

The Kubota cavitation model is sometimes called Zwart-Gerber-Belamri model or Rayleigh Plesset model. The Kubota model assumes a constant nuclei density in the fluid domain [20]. The growth and collapse of the bubble clusters are governed by the simplified Rayleigh-Plesset equation for single-bubble dynamics [39]. The cavitation process is governed by the mass transfer equation given in eq. (4), and the source and sink terms are defined as follows:

$$\dot{m}^- = C_{k_dest} \frac{3\alpha_{nuc}(1 - \alpha_v)\rho_v}{R_B} \left(\frac{2}{3} \frac{p_v - p}{\rho_l} \right)^{1/2}, \quad p < p_v \quad (7)$$

$$\dot{m}^+ = C_{k_prod} \frac{3\alpha_v \rho_v}{R_B} \left(\frac{2}{3} \frac{p - p_v}{\rho_l} \right)^{1/2}, \quad p > p_v \quad (8)$$

where α_{nuc} is the nucleation volume fraction, R_B is the bubble diameter, p_v is the saturated liquid vapor pressure, and p is the local fluid pressure. C_{k_dest} is the rate constant for vapor generated from liquid in regions where the local pressure is less than the vaporization pressure. Conversely, C_{k_prod} is the rate constant for reconversion of vapor back into liquid in regions where the local pressure exceeds the vaporization pressure. As shown in eq. (7) and (8), both the evaporation and condensation terms are assumed to be proportional to the square root of the difference between the local pressure and vapor pressure because the Kubota model was derived by assuming that the bubble dynamics are governed by the simplified Rayleigh-Plesset equation [39]. In this work,

the assumed values for the model constants are $\alpha_{nuc} = 5 \times 10^{-4}$, $R_B = 1 \times 10^{-6}$ m, $C_{k_dest} = 50$, and $C_{k_prod} = 0.01$, which are the default values in CFX [40] and are used because of their claimed general applicability.

3.3 Merkle Model

The Merkle cavitation model is sometimes called Kunz et al. model. A few researchers have adopted the Merkle model proposed by [24] (e.g., see [28, 41]), which has been presented in both the volume fraction form and the mass fraction form. It was derived primarily based on dimensional arguments for large-bubble clusters instead of individual bubbles. Consequently, the source and sink terms for the Merkle model shown in eq. (9) are directly related to the pressure difference, $p - p_v$, instead of the square root of the pressure difference as in the Kubota model:

$$\dot{m}^- = -\frac{C_{k_dest}\rho_l\rho_l\text{MIN}(p - p_v, 0)(1 - \alpha_v)}{(0.5\rho_l U_\infty^2)\rho_v t_\infty}, p < p_v \quad (9)$$

$$\dot{m}^+ = \frac{C_{m_prod}\rho_l\text{MAX}(p - p_v, 0)\alpha_v}{(0.5\rho_l U_\infty^2)t_\infty}, p > p_v \quad (10)$$

In this work, the empirical factors are set to be $C_{m_dest} = 1$ and $C_{m_prod} = 80$, which follows the constants used by Senocak and Shyy [28] for cavitating flow simulation. The mean flow time scale is defined as $t_\infty = c/U_\infty$ [19, 28] where c is the hydrofoil cord, U_∞ is equal to the inlet velocity.

As part of this work, the Merkle model is implemented in CFX by Fortran programming code. The Kubota model is also implemented by Fortran code and its results are compared to the default model results in order to verify our implementation methodology.

3.4 Turbulence Models and Turbulence Viscosity Modification

The numerical simulations presented in this paper are performed using the commercial CFD code, CFX, to solve the RANS equations. The k- ϵ and the SST (Shear Stress Transport) turbulence models are used for the cases of steady sheet cavitation and the k- ϵ and the SAS-SST turbulence models are used for the cases of unsteady sheet/cloud cavitation. In theory, the SST combines the advantages of the original k- ϵ and k- ω models by using the k- ω model near the wall, and the k- ϵ model away from the wall. The SAS-SST turbulence model basically gives the same advantages as the SST turbulence model, but the SAS-SST was designed for unsteady flow simulations. The SAS-SST turbulence model is sometimes called simply SAS turbulence model [40]. But, for this cavitation problem, it is important to test the applicability of these popular turbulence models.

It should be noted that the original RANS models were developed for fully incompressible single-phase flows and were not intended for flow problems involving compressible multiphase mixtures. To improve numerical simulations by taking into account the influence of the local compressibility effect of two-phase mixtures on turbulent closure models, Coutier-Delgosha [33] proposed to reduce the mixture turbulent viscosity of fluid at vapor/liquid interfaces based on the local vapor volume fraction α_v by substituting μ_T in eq. (3) with μ_{T_mod} :

$$f(n) = \frac{\rho_v + (1 - \alpha_v)^n(\rho_l - \rho_v)}{\rho_v + (1 - \alpha_v)(\rho_l - \rho_v)}, \mu_{T_mod} = \mu_t f(n) \quad (11)$$

The variation of the modified effective density, $\rho_{mf}(n)$, with the vapor volume fraction, α_v , for different values of n is shown in Fig. 1.

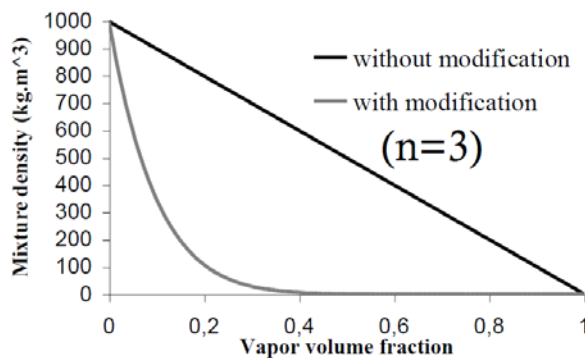


Fig. 1 Local compressibility modification of the mixture density according to eq. (11)

In [5, 25, 42], it is recommended to use $n = 3$ for the better simulation of dynamic cavitating flow around a hydrofoil, because they obtained favorable agreement between numerical and experimental results for this value.

4 Experimental Setup and Description

To validate the numerical simulation results, they are compared with experimental results of the NACA 66 hydrofoil conducted in the cavitation tunnel at the Research Institute of the French Naval Academy (Fig. 2). The test section has a cross-sectional area of 0.192 m^2 and length of 1 m. The inflow velocity ranges between 3 m/s and 15 m/s, and the pressure in the test section ranges between 30 mbar and 3 bars. The tunnel inflow turbulence intensity, defined as $V_{\infty rms}/V_\infty$ at the inlet of the test

section, is about 2%. The foil has a uniform cross-section with a NACA 66 thickness distribution with a maximum thickness-to-chord ratio of 12%, and a NACA a = 0.8 camber distribution with a maximum camber-to-chord ratio of 2%. The chord length is $c = 0.15$ m and the span length is $s = 0.191$ m. The hydrofoil is made of stainless steel, and behaved like a 2D rigid hydrofoil even though it was mounted using a cantilevered setup with a small gap (1 mm) between the free end of the hydrofoil and the test section wall. Therefore, the possible tip-vortex cavitation caused by the small gap between the hydrofoil end and the wall could not have significant influence on the mid-span section.

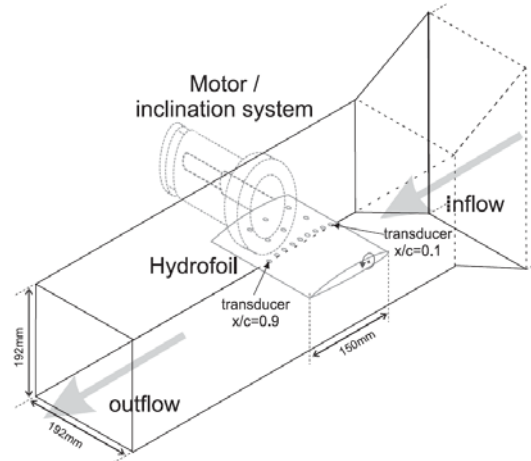


Fig. 2 Hydrofoil instrumentation and tunnel test section [43]

Pressure measurements were carried out using seventeen flush-mounted piezo-resistive transducers with a maximum pressure of 10 bars. The transducers locations were aligned along the chord on the suction side of the hydrofoil at mid-span, starting from the foil leading edge at a reduced coordinate of $x/c = 0.1$ to the trailing edge at $x/c = 0.9$, with increments of 0.1 c . Lift and drag were measured using a resistive gauge hydrodynamic balance with a range up to 1500 N in lift and 150 N in drag. Readers should refer to [3, 44] for additional details about the rigid hydrofoil experimental setup and results. The experimental results presented in this paper are taken from [3] for cases with steady sheet cavitation and from [44] for cases with unsteady sheet/cloud cavitation.

5 Numerical Setup and Description

To demonstrate and validate the numerical model, results are shown for the rigid rectangular NACA 66 hydrofoil described above. All results shown in this paper correspond to the hydrofoil at $\alpha = 6^\circ$ angle of attack and subject to a nominal free stream velocity of $V_\infty = 5$ m/s, which yields a moderate-to-high Reynolds number of $Re = V_\infty c / \nu_l = 0.75 \times 10^6$.

The density and dynamic viscosities of the liquid are taken to be $\rho_l = 997.1$ kg/m³ and $\mu_l = \rho_l \nu_l = 0.890 \times 10^{-3}$ Pa·s, respectively, which correspond to fresh water at 25°C. The vapor density is $\rho_v = 0.02308$ kg/m³ and the vapor viscosity is $\mu_v = 9.8626 \times 10^{-6}$ Pa·s. The vapor pressure of water at 25°C is $p_v = 3169$ Pa.

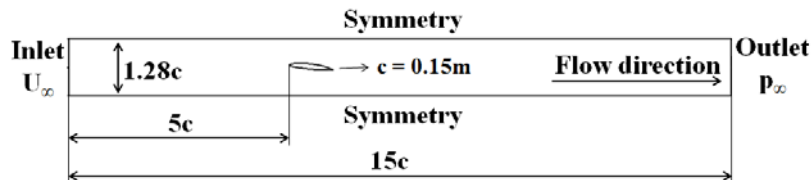


Fig. 3 Fluid domain and boundary conditions

Based on the experimental observations of cavitating flow over the 3D rectangular hydrofoil [45], the flow is found to be approximately uniform over 80 to 90% of the foil in the spanwise direction. Hence, for computational efficiency, a 2D analysis is applied in this work. The 2D fluid domain is shown in Fig. 3, which corresponds to the height of the experimental test section. The computational domain has an extent of about 5 c upstream and 10 c downstream of the foil to simulate near-infinite boundary conditions at the inlet and outlet. Although the boundary layer growth may affect the flow at the foil and the turbulence intensity may change to a different extend if the inlet is too far, the inlet cannot be set at the same distance upstream as the experiment because the exact parabolic velocity profile cannot be found in the experimental papers. A no-slip boundary condition is imposed on the hydrofoil surface. Symmetry conditions are imposed on the top and bottom boundaries of the tunnel because our tested simulations with the symmetry conditions and the wall conditions on these boundaries gave the same results for this case. Moreover, the use of the symmetry conditions allows to not concentrate the mesh near the top and the bottom; this helps to optimize the mesh and the simulation time. The inlet velocity is set to be $V_\infty = 5$ m/s and the outlet pressure is set to vary according to the cavitation number, defined as $\sigma = (p_\infty - p_v) / (0.5 \rho_l V_\infty^2)$, where p_∞ is the tunnel pressure. This p_∞ is used to set the pressure outlet boundary condition. A constant turbulent intensity of 2% is set at the inlet boundary and is equal to the experimentally measured turbulent intensity.

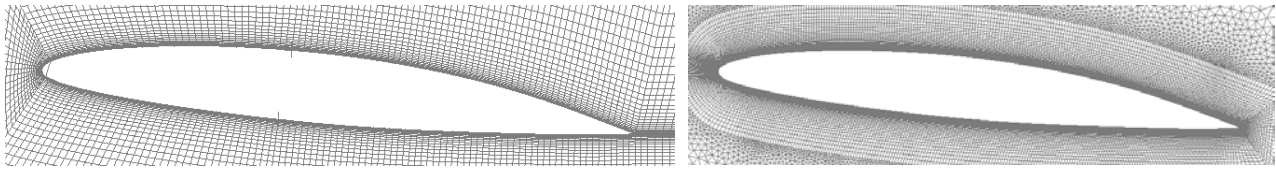


Fig. 4 Fluid mesh details (structured mesh: left, hybrid mesh: right)

All cavitating runs have been initialized with a fully wetted simulation or non-cavitating simulation to avoid any vapor fraction. The tunnel outlet pressure is then decreased progressively until the particular cavitation number is reached. Various fully structured meshes were generated using ICEM, corresponding to various values of y^+ where $y^+ = yu_\tau/\nu_1$, y is the thickness of the first cell from the foil surface, and u_τ is the wall frictional velocity. The results from mesh independence tests for various values of y^+ and various mesh expansion factors around the hydrofoil are presented in section 6. Hybrid meshes generated by an in-house mesh generator are composed of 70 000 nodes with 50 structured nodes across the foil boundary layer, which is selected to ensure $y^+ = 1$. In the hybrid meshes, the regions outside the boundary layer have been discretized with unstructured triangular elements. Mesh refinements are performed at the foil leading edge, trailing edge, and in the wake region (Fig. 4). The spatial derivatives are computed using a second-order upwind scheme.

6 Numerical Results and Analysis

There are two test cases: steady sheet cavitation and unsteady sheet/cloud cavitation that are used to perform CFD multiphase cavitation simulations. The first case study is for the cavitation number 1.49 and the second one is for the cavitation number 1.00.

6.1 Steady Sheet Cavitation

In this part, the steady sheet flow cavitation is studied to understand the influence of different factors: mesh density, mesh type, turbulence model, cavitation model, and turbulence viscosity. The predicted surface pressure coefficients from numerical simulations, $C_p = (P - P_\infty)/(0.5\rho V_\infty^2)$, will be compared with the measured values for each set of studied numerical factors.

6.1.1 Mesh Analysis

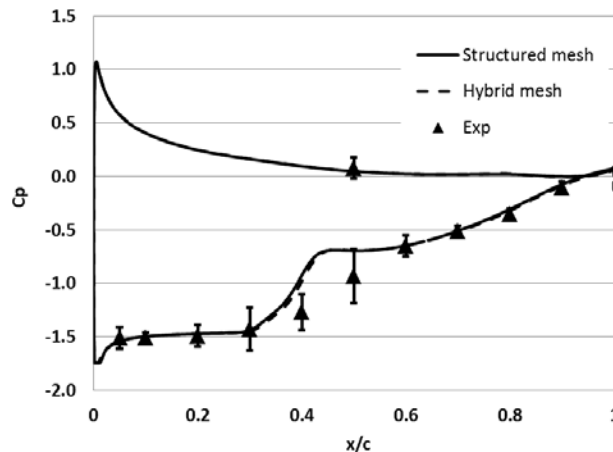


Fig. 5 Comparisons of the measured versus predicted pressure coefficients obtained using different types of mesh with $y^+ = 1$, Kubota cavitation model, k- ϵ turbulence model, no turbulence viscosity modification

The structured and hybrid types of mesh are studied using Kubota cavitation model and the k- ϵ turbulence model, without turbulence viscosity modification (Fig. 5). The two types of mesh give the same numerical results for the surface pressure coefficients on the hydrofoil. This result proves the good applicability of hybrid meshes for cavitating flow simulation, especially for complicated geometries where it is easier to generate hybrid meshes with different mesh concentration zones. But, for the simple geometry case of this study, the structured meshes can be easily generated. Therefore, the fully structured meshes will be applied for subsequent simulation results presented in this paper.

In order to understand the influence of mesh density around the hydrofoil on cavitating flow simulation results, the mesh expansion factor and the non-dimensional wall distance (y^+) were selected to be studied with different values as follows: ratio = 1.05 ($y^+ = 0.5, y^+ = 1, y^+ = 30$), ratio = 1.1 ($y^+ = 0.5, y^+ = 1, y^+ = 30$), ratio = 1.2 ($y^+ = 0.5, y^+ = 1, y^+ = 30$), using structured mesh type, Kubota cavitation model and the k- ϵ turbulence model, without turbulence viscosity modification. No significant difference on the numerical surface pressure distribution was found. One of the results is shown in the Fig. 5 (structured mesh curve).

6.1.2 Effect of Turbulence Model

The influence of different turbulence models k- ϵ and SST is studied for the Kubota cavitation model and the Merkle cavitation model, using a structured mesh with $y^+ = 1$, without turbulence viscosity modification (Fig. 6). The predicted surface pressure coefficients, $C_p = (P - P_\infty)/(0.5\rho V_\infty^2)$, are shown along with the measured values.

For the Kubota cavitation model presented on the left hand side of Fig. 6, the numerical simulation results of both turbulence models are able to fall within the error bars for nine out of ten pressure points studied on the upper part of the foil. The only exception is at the point $x/c = 0.4$ inside the closure region of the cavitation region. In this region, the flow turbulence is stronger

than elsewhere, as observed through the figures of turbulent kinetic energy (Table 1). The comparison of different turbulence models in Fig. 6 shows that the predicted numerical results around this region can be improved by a turbulence model more suitable to cavitating flow. For this case, the k- ϵ model has given numerical results closer to experimental data around the cavitation closure regions than the SST turbulence model.

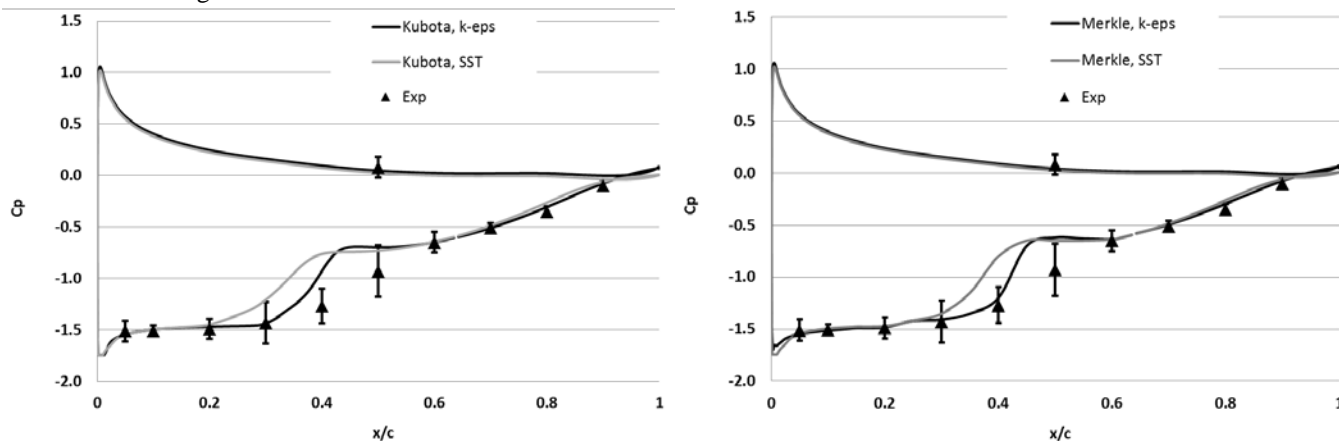


Fig. 6 Comparisons of measured versus predicted pressure coefficients obtained for different turbulence models with Kubota cavitation model (left) and Merkle cavitation model (right), no turbulence viscosity modification

For the Merkle cavitation model presented on the right hand side of Fig. 6, the numerical simulation results using the SST model are able to fall within the error bars of eight out of ten pressure points studied on the upper part of the foil, except at the point $x/c = 0.4$ and $x/c = 0.5$ inside the closure region of cavitation bubbles. The numerical simulation results of the k- ϵ model fall within the error bars for nine out of ten pressure points studied on the upper part of the foil. In fact, the predicted values for these nine points are quite close to the center of the value range measured and indicated by the error bars. The exception is at the point $x/c = 0.5$ inside the closure region of the cavitation region, but the numerical result is close to the error bar of the experimental result.

6.1.3 Effect of Cavitation Model

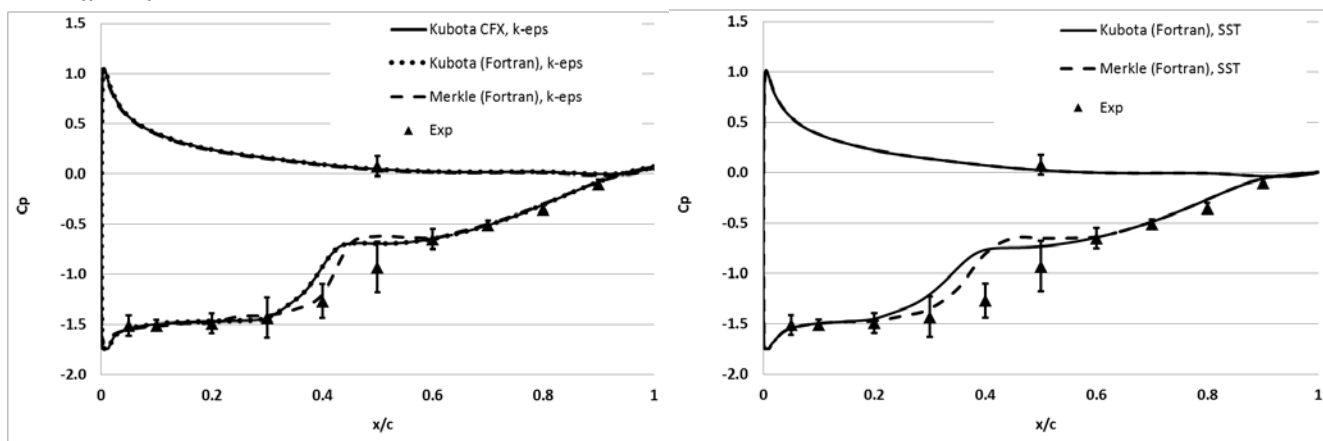


Fig. 7 Comparisons of measured versus predicted pressure coefficients obtained for different cavitation models using k- ϵ turbulence model (left) and SST turbulence model (right), no turbulence viscosity modification

For the k- ϵ turbulence model, different cavitation models, the default CFX Kubota cavitation model, the Kubota cavitation model coded by User Fortran, and the Merkle cavitation model coded by User Fortran are studied without turbulence viscosity modification. As shown on the left hand side of Fig. 7, for the surface pressure coefficient distribution on the hydrofoil, the Kubota model coded by User Fortran gave the same results as the default CFX Kubota cavitation model. This result verifies our implementation methodology for cavitation models in the solver CFX. In comparison to the Kubota model, the Merkle cavitation model has shown numerical results slightly closer to the experimental data in the region around the pressure point $x/c = 0.4$. In contrast, the Merkle result at the pressure point $x/c = 0.5$ is a bit farther from the experimental data than the Kubota result. For the rest of the surface pressure coefficient distribution, both cavitation models gave exactly the same results.

For the SST turbulence model, the Kubota and Merkle cavitation model results are presented on the right hand side of Fig. 7. Both cavitation models are able to give numerical results reaching nine out of ten uncertainty bars of the experimental data. The Merkle curve is a bit closer to the experimental curve at $x/c = 0.4$, in contrast, a bit farther from the experimental curve at the region around $x/c = 0.5$.

The question arises, why does the Merkle model give slightly better results than the Kubota model? First of all, the numerical prediction quality of cavitation closure regions depends on the condensation term representing the collapse process of the cavitation phenomenon. Looking back at the mathematical formulas of the cavitation models, the condensation term of the Merkle model is proportional to the pressure difference, $p - p_v$, instead of the square root of the pressure difference as in the Kubota

model. This is the main difference of the two cavitation models. However, why a cavitation model directly proportional to the pressure difference gives slightly better results than a cavitation model proportional to the square root of the pressure difference for this case study? This relationship between the improvements given by the Merkle model and its mathematical formulas is still unknown.

6.1.4 Turbulent Viscosity Modification

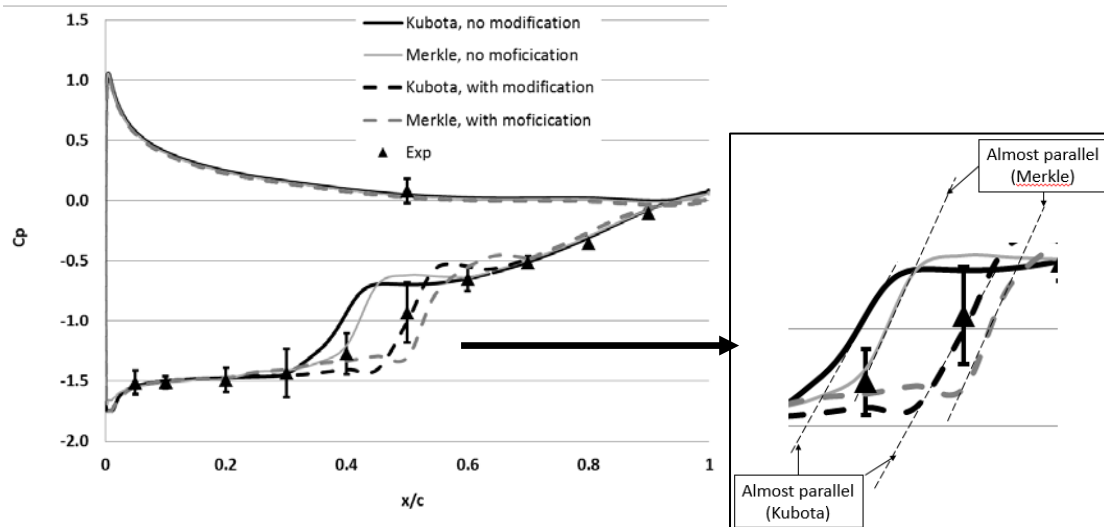


Fig. 8 Comparisons of the measured versus predicted pressure coefficients with and without turbulence viscosity modification, different cavitation models, k-ε turbulence model

The effect of turbulent viscosity modification for each cavitation model is studied in order to understand the influence of local compressibility at the vapor/liquid interfaces on the numerical simulation results. The cases with and without turbulence viscosity modification are compared using Kubota and Merkle cavitation models, structured mesh $y^+ = 1$ and k-ε turbulence model (Fig. 8). The predicted surface pressure coefficients, $C_p = (P - P_\infty)/(0.5\rho V_\infty^2)$, are shown along with the measured values. In comparison to the case without turbulence viscosity modification, the modification of turbulence viscosity shows that the numerical pressure coefficient distribution is closer to the experimental data for the pressure points around $x/c = 0.4$ and $x/c = 0.5$. However, for the pressure points around $x/c = 0.6$, the modification of turbulence viscosity made the predicted pressure coefficients a bit farther from the experimental data. This means that the indirect way of considering the cavitation compressibility by modifying the turbulence viscosity recommended by Coutier-Delgosha [33] has shown good performance for this case study. This method of reducing the turbulence viscosity at the vapor/liquid interfaces helps to slow the numerical collapse process down. Therefore, the predicted cavitation region is longer, which makes the numerical pressure coefficients around the closure region fit better the experimental data.

On the right hand side of Fig. 8, there is a zoom of the regions where the numerical results are affected by the modification of the turbulence viscosity. The change in surface pressure coefficients inside this region is found to be shifted towards the hydrofoil trailing edge, and in parallel to the original curves for each cavitation model. This finding helps understand clearly the effect of the technique of turbulent viscosity modification based on the mixture density at the vapor/liquid interfaces on the predicted surface pressure coefficients, as described above.

Table 1 Comparison of the vapor fraction and turbulence kinetic energy contours with and without turbulence viscosity modification, for two different cavitation models, k-ε turbulence model; volume fraction: black (pure water), white (pure vapor); turbulent kinetic energy: black (highest value), white (lowest value)

	Kubota model	Merkle model
No turbulence viscosity modification Volume fraction		
No turbulence viscosity modification Turbulent kinetic energy		
With turbulence viscosity modification Volume fraction		
With turbulence viscosity modification Turbulent kinetic energy		

Table 1 shows the predicted vapor volume fraction and turbulent kinetic energy obtained using the Kubota and the Merkle cavitation models, with and without turbulent viscosity modification. The vapor fraction contours for the two different cavitation models with and without turbulent viscosity modification are, respectively, shown in the first and third rows in Table 1; the black color corresponds to pure water, whereas the white color corresponds to pure vapor. The corresponding turbulent kinetic energy contours are shown in the second and fourth rows in Table 1, where the lowest turbulent kinetic energy is shown in white, and the highest turbulent kinetic energy is shown in black.

For the cases without turbulent viscosity modification, the two cavitation models yield different levels of turbulent kinetic energy in the cavitation regions and at the cavitation closure region, which in turn modified the vapor volume fraction and cavitation shape, as shown in the first two rows of Table 1. The Merkle model has a lower level of turbulent kinetic energy in the cavitation region, which leads to a longer sheet cavity.

For the cases with turbulent viscosity modification, the results for the two models in the bottom two rows of Table 1 show a general decrease in the turbulent kinetic energy in the vapor region, compared to the cases without turbulent viscosity modification. The results show that the mixture density-based correction to the turbulent viscosity at the vapor/liquid interfaces has different degrees of impact on the two cavitation models. The Merkle model predicts similar cavity lengths for the cases with and without the turbulence viscosity modification. The Kubota model shows a significant increase in cavity length at the cavity trailing edge with the modification. The dynamics of the predicted cavitation regions are well correlated to the performance of the predicted pressure coefficients on the hydrofoil presented in Fig. 8. This finding also shows that the turbulent viscosity is over-predicted by the original turbulence models without turbulent viscosity modification tested in this study for cavitating flow simulations and it should be modified by a turbulent viscosity modification technique like the method presented in this paper.

6.2 Unsteady Sheet/Cloud Cavitation

6.2.1 Prediction of Pressure Fluctuations

To evaluate the prediction quality of the two different cavitation models for unsteady sheet/cloud cavitation, results are shown for the case with $\sigma = 1.00$, $Re = 750\,000$ and $\alpha = 6^\circ$.

For the timestep selection, in the theory of unsteady flow simulation, it is recommended to choose a timestep corresponding to an average CFL number around 1. As $CFL = U_\infty \Delta t / \Delta x$, so for this case study, the timestep should be around 1×10^{-4} to correspond to a CFL of 1. This timestep was tested several times for this case, but the simulations did not converge, firstly due to the high unsteadiness of the unsteady sheet/cloud cavitation regime, and secondly due to the interaction between the User Fortran programming code and the solver, CFX. Therefore, the timestep had to be increased until the simulations converged. In order to obtain the highest possible precision, the smallest usable timestep for this case was found to be about $\Delta t = 1 \times 10^{-2}$ s, corresponding to the CFL number around 100. This issue can also occur for other highly unsteady flow simulations in different fields, for example, fluid/structure interaction simulation. This important point would need more research in numerical algorithms for improving the numerical convergence in the future.

Based on available experimental data presented in [44], an analysis of hydrofoil suction side load can be calculated by summing the product of the pressure coefficients with length elements along the surface, which was calculated as follows in the experimental study:

$$C_l^+(t) = \sum_{i=1}^{10} C_p \left(\frac{x_i}{c}, t \right) \Delta \left(\frac{x_i}{c} \right) \quad (12)$$

where $C_p(x_i/c, t)$ is the pressure coefficient at location x_i/c and $\Delta(x_i/c) = 0.1$ is the non-dimensional distance between two consecutive pressure transducers. For comparison purposes, the same procedure is applied to the CFD results. It should be noted that since the flow is mostly attached along the pressure side, the changes to the total lift coefficient should be affected mainly by the suction side dynamics, which is represented by the suction side lift coefficient.

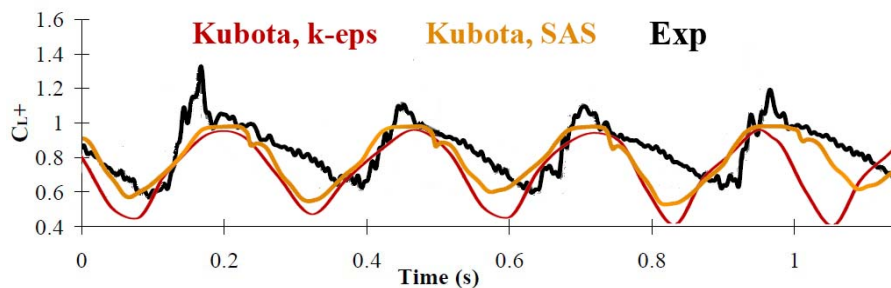


Fig. 9 Comparisons of the measured and the predicted suction side lift coefficients obtained using Kubota cavitation model, with k- ϵ and SAS-SST turbulence models

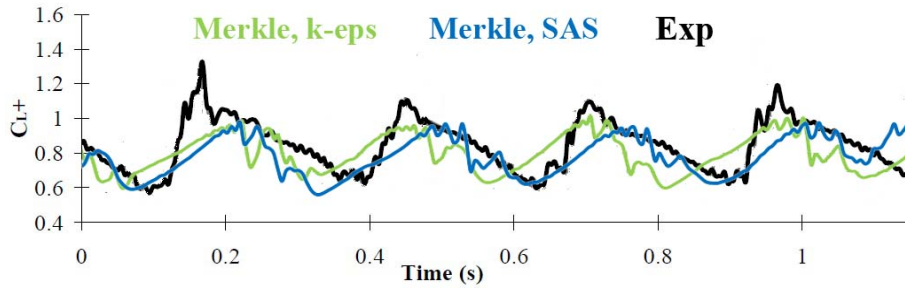


Fig. 10 Comparisons of the measured and the predicted suction side lift coefficients obtained using Merkle cavitation model, with k- ϵ and SAS-SST turbulence models

Comparisons of the predicted and measured suction side lift coefficients are shown in Fig. 9 for Kubota cavitation model and in Fig. 10 for Merkle cavitation model with k- ϵ and SAS-SST turbulence models. A fair comparison is observed between the experimental measurements and numerical predictions obtained with both the Kubota and the Merkle cavitation models.

For both cavitation models, the cycle of the lift fluctuations has been predicted quite well. However, the mean values of the lift coefficient amplitudes are not well predicted by any cavitation model tested. For the mean values of the coefficients, the values from the two cavitation models are lower than experimental data by around 0.1 to 0.2 units of lift coefficient. The Merkle cavitation model curve shows more dynamic behavior similar to the experimental curve than the Kubota one.

For the cases with Kubota cavitation model, in comparison with the k- ϵ turbulence model, the SAS-SST model is found to show slightly more dynamic behavior of the sheet/cloud cavitation. The simulations with the SAS-SST turbulence model predict the frequency of the lift fluctuations on the hydrofoil closer to the experimental data than with the k- ϵ turbulence model (Table 2). Moreover, the curve of SAS-SST model predicts the minimum value of the lift fluctuations on the hydrofoil slightly closer to the experimental data than the k- ϵ model one, as seen in Fig. 9.

For the cases with the Merkle cavitation model, the simulations with the SAS-SST turbulence model predict the frequency of the lift fluctuations on the hydrofoil slightly closer to the experimental data than with the k- ϵ turbulence model (Table 2). The mean value, maximum value and minimum value predicted by the two turbulence models are almost the same. The maximum value of the lift fluctuations are not well predicted by any turbulence model tested.

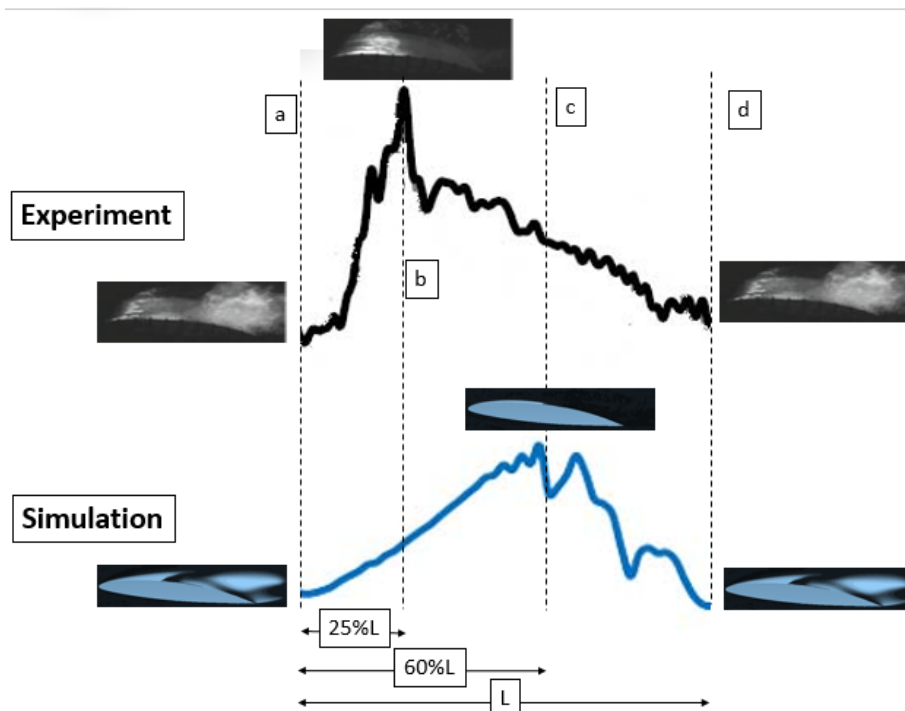


Fig. 11 Comparisons of the measured and the predicted suction side lift coefficients obtained for one cavitation shedding cycle

Fig. 11 presents a zoom for the measured and predicted lift coefficients obtained for one cavitation shedding cycle. Physically, the larger cavitation bubbles are, the lower the lift coefficient generated on the hydrofoil is. This physical phenomenon is also found by the numerical simulations. However, the peak of the predicted lift fluctuations is found at around 60% of the cavitation shedding cycle, which is different from the experimental observation, at around 25% of the cavitation shedding cycle. This means that the numerical evaporation process should be longer and the numerical collapse should be shorter.

The accuracy of the two tested cavitation models for predicting the lift coefficient fluctuations of this complex sheet/cloud cavitation simulation is still insufficient for predicting the pressure fluctuations on the hydrofoil during one shedding cavitation cycle. The technique of cavitating flow simulation should be improved in the future in order to be able to capture better the dynamics of this case.

6.2.2 Prediction of Cavitation Vapor

Fig. 12 shows the comparisons between the predicted vapor fraction obtained using the Kubota and the Merkle models with experimental visualizations presented in [44] for the operating condition $\sigma = 1.00$, $Re = 750\,000$, $\alpha = 6^\circ$. The predicted cavity behavior obtained using the Merkle model is generally in better agreement with the experiments than the Kubota model. The $k-\epsilon$ and SAS-SST turbulence models do not show significant difference for the visualization of cavitation bubbles. As shown in Fig. 12, a stable leading edge sheet cavity gradually expands towards the foil trailing edge between times t_1 to t_3 . The upstream motion of the re-entrant jet can be observed at times t_3 and t_4 in Fig. 12 (a and b). The clockwise vorticity generated by the re-entrant jet causes the cavity to roll up and partially sheds at times t_4 and t_5 and is supported by the foamy appearance of the cavity trailing edge in Fig. 12 (c). At time t_6 , the sheet cavity mostly sheds; the cavity flows downstream and forms a cloud cavity, which can be seen at time t_7 . The Merkle cavitation model seems to show more dynamic behavior like in the experimental figures than the Kubota cavitation model. Especially from t_4 to t_7 , slightly more cloud vapor is simulated by the Merkle than by the Kubota model.
















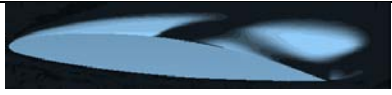




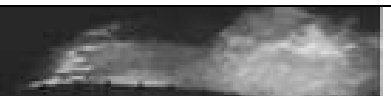
Vapor fraction Kubota Model (a)	Vapor fraction Merkle Model (b)	Experiments (c)
		
t1 = 20% Cycle		
		
t2 = 36% Cycle		
		
t3 = 52% Cycle		
		
t4 = 60% Cycle		
		
t5 = 68% Cycle		
		
t6 = 76% Cycle		
		
t7 = 84% Cycle		

Fig. 12 Comparisons of the predicted vapor fraction contours predicted using the Kubota and Merkle cavitation model with experimental observations, $k-\epsilon$ turbulence model

6.2.3 Effect of the Turbulent Viscosity

In this part, the turbulence viscosity modification is analyzed for taking into account the local compressibility at the vapor/liquid interfaces for the cases of unsteady sheet/cloud cavitation. As seen in Table 2, for the two cavitation models, the cavity shedding frequency predicted by SAS-SST turbulence model is closer to the experimental data than that predicted by the $k-\epsilon$ turbulence model. With the turbulence viscosity modification, the frequencies are found to be closer to the measured value because the turbulence viscosity modification helps to make the evaporation process a bit longer for both cavitation models. The Merkle cavitation model is found to predict the shedding frequency slightly closer to the experimental data.

Table 2 Comparison of the measured and predicted cavity shedding frequencies (Hz) for the Kubota and Merkle cavitation models with $n = 1$ and $n = 3$ for the case of unsteady sheet/cloud cavitation

	Kubota model		Merkle model		Experiments
	No turbulence viscosity modification	With turbulence viscosity modification	No turbulence viscosity modification	With turbulence viscosity modification	
k-ε model	4.0	3.5	4.1	3.6	3.5
SAS-SST model	3.7	3.4	3.8	3.4	3.5

7 Conclusions

The applicability of two cavitation models, Kubota and Merkle, is studied for the cavitating flow simulation around a NACA66 hydrofoil at $\alpha = 6^\circ$, $Re = 750\,000$ for two cavitation regimes: steady partial sheet cavitation ($\sigma = 1.49$) and unsteady sheet/cloud cavitation ($\sigma = 1.00$). Mesh analysis including the effects of mesh types, mesh expansion factors around the hydrofoil and distances from hydrofoil wall to first mesh node has been considered carefully. The effects of turbulence models on the cavitating flow dynamics for different cavitation models are analyzed. The influence of local compressibility based on turbulent viscosity modification is considered. The relationship between the turbulent viscosity modification and the cavitating flow simulation results has been clarified throughout the paper.

For the cases of steady sheet cavitation regime ($\sigma = 1.49$), the numerical models have shown good results in comparison with experimental data. The k-ε model has given pressure distributions slightly closer to the experimental data than the SST turbulence model for this case study. The hybrid meshes have performed very well for these cavitating simulations, giving the same results as the structured meshes. The Merkle cavitation model has been found to predict the pressure distributions slightly closer to the experimental data than the Kubota cavitation model for this case. Our results on modifying the turbulent viscosity on the mixture vapor/liquid zones have shown good improvement for cavitating flow simulation. However, the current cavitation simulation technique is still limited. The prediction quality for the numerical surface pressure coefficients at the cavitation closure regions is not yet sufficient even with the turbulent viscosity modification.

For the cases of unsteady sheet/cloud cavitation ($\sigma = 1.00$), the frequencies of the suction side lift coefficients predicted using the Kubota and Merkle cavitation models are quite close to experimental measurements. The mean values of the suction side lift coefficients are found lower than the experimental data with a gap of 0.1 to 0.2 lift coefficient unit. The maximum amplitude of the suction side lift coefficients is not yet obtained by the current numerical methods. The peak location of lift fluctuations are found at 60% of the cavitation shedding cycle which is different from the 25% value of the experimental measurement. The predicted cavitation bubbles obtained by the tested cavitation models look similar to the experimental visualizations. The Merkle cavitation model is found to give more dynamic behavior on the suction side lift coefficients than the Kubota model. No clear explanation for this advantage of the Merkle cavitation model has been found for this highly unsteady sheet/cloud cavitation regime.

The limitations of the current cavitating flow simulation technique for this highly unsteady cavitating flow regime are found as follows. Firstly, the flow simulations diverge with standard unsteady simulation timesteps. Secondly, the prediction quality of current cavitation models is not yet sufficient for predicting the cavitation patterns. Moreover, the fact of adding the Merkle cavitation model by User Fortran code makes the numeric convergence very difficult, especially for this complex shedding unsteady sheet/cloud cavitation. Please note that the modification of turbulence viscosity makes the simulation also harder to converge. Generally, the convergence is better with bigger timesteps than with smaller timesteps. This numeric problem would need more efforts to improve the convergence in the future.

Nomenclature

c	hydrofoil chord (m)	α	void ratio
C_p	pressure coefficient ($= (p-p_\infty)/(0.5\rho v_\infty^2)$)	ε	dissipation rate
k	turbulent kinetic energy (m^2/s^2)	μ, μ_t	molecular and eddy viscosity
Re	Reynolds number ($= u_\infty c/\nu$)	ν	fluid kinematic viscosity ($= \mu/\rho$)
\dot{m}^+, \dot{m}^-	source term and sink term	ρ	fluid density
p, P	local fluid pressure	σ	cavitation number
p_v	vaporization pressure		
P_∞	reference pressure	$(\cdot)_i, (\cdot)_j, (\cdot)_k$	directions of the Cartesian coordinates
u_τ	friction velocity	$(\cdot)_v, (\cdot)_l, (\cdot)_m$	vapor value, liquid value and mixture value
U_∞	free stream velocity	$(\cdot)_T$	turbulent value
u	local fluid velocity		
y^+	dimensionless wall distance ($= yu_\tau/\nu$)		

References

- [1] Tran, T. D., Nennemann, B., Vu, T. C., and Guibault, F., 2014, "Numerical Simulation of Cavitating Flow around a Hydrofoil," eds., Chicago, Illinois, USA,
- [2] Tran, T. D., Nennemann, B., Vu, T. C., and Guibault, F., 2014, "Numerical Simulation of Unsteady Sheet/Cloud Cavitation," eds., Montreal, Canada,
- [3] Leroux, J.-B., Astolfi, J. A., and Billard, J. Y., 2004, "An Experimental Study of Unsteady Partial Cavitation," Journal of Fluids Engineering, Transactions of the ASME, 126(1), pp. 94-101.

- [4] Reisman, G. E., Wang, Y. C., and Brennen, C. E., 1998, "Observations of Shock Waves in Cloud Cavitation," *Journal of Fluid Mechanics*, 355(pp. 255-83).
- [5] Huang, B., Young, Y. L., Wang, G., and Shyy, W., 2013, "Combined Experimental and Computational Investigation of Unsteady Structure of Sheet/Cloud Cavitation," *Journal of Fluids Engineering*, 135(7), pp. 071301-071301.
- [6] Barre, S., Rolland, J., Boitel, G., Goncalves, E., and Patella, R. F., 2009, "Experiments and Modeling of Cavitating Flows in Venturi: Attached Sheet Cavitation," *European Journal of Mechanics - B/Fluids*, 28(3), pp. 444-464.
- [7] Stutz, B., and Reboud, J. L., 1997, "Experiments on Unsteady Cavitation," *Experiments in Fluids*, 22(3), pp. 191-8.
- [8] Arndt, R. E. A., 2012, "Some Remarks on Hydrofoil Cavitation," *Journal of Hydrodynamics*, 24(3), pp. 305-314.
- [9] Franc, J.-P., 1995, *La Cavitation: Mécanismes Physiques Et Aspects Industriels*, Grenoble : Presses universitaires de Grenoble.
- [10] Arndt, R. E. A., 2012, "Cavitation Research from an International Perspective," eds., Beijing, China, 15.
- [11] Kubota, A., Kato, H., Yamaguchi, H., and Maeda, M., 1989, "Unsteady Structure Measurement of Cloud Cavitation on a Foil Section Using Conditional Sampling Technique," *Journal of Fluids Engineering*, 111(2), pp. 204-210.
- [12] Kravtsova, A. Y., Markovich, D. M., Pervunin, K. S., Timoshevskiy, M. V., and Hanjalić, K., 2014, "High-Speed Visualization and Piv Measurements of Cavitating Flows around a Semi-Circular Leading-Edge Flat Plate and Naca0015 Hydrofoil," *International Journal of Multiphase Flow*, 60(0), pp. 119-134.
- [13] Tseng, C.-C., and Shyy, W., 2010, "Modeling for Isothermal and Cryogenic Cavitation," *International Journal of Heat and Mass Transfer*, 53(1-3), pp. 513-525.
- [14] Morgut, M., Nobile, E., and Bilus, I., 2011, "Comparison of Mass Transfer Models for the Numerical Prediction of Sheet Cavitation around a Hydrofoil," *International Journal of Multiphase Flow*, 37(6), pp. 620-626.
- [15] Utturkar, Y., Wu, J., Wang, G., and Shyy, W., 2005, "Recent Progress in Modeling of Cryogenic Cavitation for Liquid Rocket Propulsion," *Progress in Aerospace Sciences*, 41(7), pp. 558-608.
- [16] Delannoy, Y., and Kueny, J. L., 1990, "Two Phase Flow Approach in Unsteady Cavitation Modelling," eds., Toronto, Ont, Can, 98.
- [17] Chen, Y., and Heister, S. D., 1996, "Modeling Hydrodynamic Nonequilibrium in Cavitating Flows," *Journal of Fluids Engineering, Transactions of the ASME*, 118(1), pp. 172-178.
- [18] Gopalan, S., and Katz, J., 2000, "Flow Structure and Modeling Issues in the Closure Region of Attached Cavitation," *Physics of Fluids*, 12(4), pp. 895-911.
- [19] Senocak, I., and Shyy, W., 2002, "Evaluation of Cavitation Models for Navier-Stokes Computations," eds., Montreal, Que., United states, 257.
- [20] Kubota, A., Kato, H., and Yamaguchi, H., 1992, "A New Modelling of Cavitating Flows: A Numerical Study of Unsteady Cavitation on a Hydrofoil Section," *Journal of Fluid Mechanics*, 240(pp. 59-96).
- [21] Kunz, R. F., Boger, D. A., Stinebring, D. R., Chyczewski, T. S., Lindau, J. W., Gibeling, H. J., Venkateswaran, S., and Govindan, T. R., 2000, "A Preconditioned Navier-Stokes Method for Two-Phase Flows with Application to Cavitation Prediction," *Computers & Fluids*, 29(8), pp. 849-75.
- [22] Singhal, A. K., Athavale, M. M., Huiying, L., and Yu, J., 2002, "Mathematical Basis and Validation of the Full Cavitation Model," *Transactions of the ASME. Journal of Fluids Engineering*, 124(3), pp. 617-24.
- [23] Decaix, J., 2013, "Modélisation Et Simulation De La Turbulence Compressible En Milieu Diphasique : Application Aux Écoulements Cavitants Instationnaires," Ph.D. thesis, Grenoble university,
- [24] Merkle, C. L., Feng, J. Z., and Buelow, P. E. O., 1998, "Computational Modeling of the Dynamics of Sheet Cavitation," eds., Grenoble, France,
- [25] Huang, B., Ducoin, A., and Young, Y. L., 2012, "Evaluation of Cavitation Models for Prediction of Transient Cavitating Flows around a Stationary and a Pitching Hydrofoil," eds., Singapore,
- [26] Saito, Y., Nakamori, I., and Ikoha, G., 2003, "Numerical Analysis of Unsteady Vaporous Cavitating Flow around a Hydrofoil," eds., Osaka, Japan,
- [27] Vortmann, C., Schnerr, G. H., and Seelecke, S., 2003, "Thermodynamic Modeling and Simulation of Cavitating Nozzle Flow," *International Journal of Heat and Fluid Flow*, 24(5), pp. 774-783.
- [28] Senocak, I., and Shyy, W., 2002, "A Pressure-Based Method for Turbulent Cavitating Flow Computations," *Journal of Computational Physics*, 176(2), pp. 363-383.
- [29] Biao, H., Ducoin, A., and Yin Lu, Y., 2013, "Physical and Numerical Investigation of Cavitating Flows around a Pitching Hydrofoil," *Physics of Fluids*, 25(10), pp. 102109 (27 pp.).
- [30] Charrière, B., Decaix, J., and Goncalves, E., 2015, "A Comparative Study of Cavitation Models in a Venturi Flow," *European Journal of Mechanics - B/Fluids*, 49, Part A(0), pp. 287-297.
- [31] Goncalves, E., 2014, "Modeling for Non Isothermal Cavitation Using 4-Equation Models," *International Journal of Heat and Mass Transfer*, 76(pp. 247-262).
- [32] Goncalves, E., and Charrière, B., 2014, "Modelling for Isothermal Cavitation with a Four-Equation Model," *International Journal of Multiphase Flow*, 59(pp. 54-72).
- [33] Coutier-Delgosha, O., Fortes-Patella, R., and Reboud, J. L., 2003, "Evaluation of the Turbulence Model Influence on the Numerical Simulations of Unsteady Cavitation," *Journal of Fluids Engineering, Transactions of the ASME*, 125(1), pp. 38-45.
- [34] Huang, B., Ducoin, A., and Young, Y. L., 2013, "Physical and Numerical Investigation of Cavitating Flows around a Pitching Hydrofoil," *Physics of Fluids*, 25(10), pp.
- [35] Ji, B., Luo, X. W., Arndt, R. E. A., Peng, X., and Wu, Y., 2015, "Large Eddy Simulation and Theoretical Investigations of the Transient Cavitating Vortical Flow Structure around a Naca66 Hydrofoil," *International Journal of Multiphase Flow*, 68(0), pp. 121-134.
- [36] Bensow, R. E., and Bark, G., 2010, "Implicit Les Predictions of the Cavitating Flow on a Propeller," *Journal of Fluids*

Engineering, 132(4), pp. 041302-041302.

- [37] Roohi, E., Zahiri, A. P., and Passandideh-Fard, M., 2013, "Numerical Simulation of Cavitation around a Two-Dimensional Hydrofoil Using Vof Method and Les Turbulence Model," *Applied Mathematical Modelling*, 37(9), pp. 6469-6488.
- [38] Launder, B. E., and Spalding, D. B., 1974, "The Numerical Computation of Turbulent Flows," *Computer Methods in Applied Mechanics and Engineering*, 3(2), pp. 269-89.
- [39] Brennen, C. E., 2005, *Fundamentals of Multiphase Flow*, Cambridge University Press,
- [40] Ansys, 2012-10, *Ansys Cfx Tutorials 14.5*,
- [41] Ducoin, A., Biao, H., and Yin Lu, Y., 2012, "Numerical Modeling of Unsteady Cavitating Flows around a Stationary Hydrofoil," *International Journal of Rotating Machinery*, pp. 215678 (17 pp.).
- [42] Ducoin, A., Huang, B., and Young, Y. L., 2012, "Numerical Modeling of Unsteady Cavitating Flows around a Stationary Hydrofoil," *International Journal of Rotating Machinery*, 2012(pp. 1-17.
- [43] Ducoin, A., Astolfi, J. A., Deniset, F., and Sigrist, J. F., 2009, "Computational and Experimental Investigation of Flow over a Transient Pitching Hydrofoil," *European Journal of Mechanics, B/Fluids*, 28(6), pp. 728-43.
- [44] Leroux, J.-B., Coutier-Delgosha, O., and Astolfi, J. A., 2005, "A Joint Experimental and Numerical Study of Mechanisms Associated to Instability of Partial Cavitation on Two-Dimensional Hydrofoil," *Physics of Fluids*, 17(5), pp. 1-20.
- [45] Wang, G., Senocak, I., Shyy, W., Ikohagi, T., and Cao, S., 2001, "Dynamics of Attached Turbulent Cavitating Flows," *Progress in Aerospace Sciences*, 37(6), pp. 551-581.